The swelling of cellulose foams due to liquid transport

Morad Mirzajanzadeh, Vikram S. Deshpande, Norman A. Fleck*

Engineering Department, Cambridge University, Trumpington Street, Cambridge CB2 1PZ, UK

Abstract

Cellulose-based foams are available commercially in a dry pre-compressed state, but can swell upon infiltration by a suitable liquid. A series of experiments reveal that pre-compressed foams can swell in one direction by an order of magnitude when infiltrated by water or glycerol; in contrast, no swelling accompanies infiltration by ethanol. The kinetics (and underlying mechanisms) of infiltration and of swelling are quantified by a series of critical experiments on both pre-compressed foam and pre-expanded foam, using water, glycerol and ethanol. Infiltration is driven by capillarity, cell wall diffusion and by opening of capillaries during swelling of the foam. Ethanol-infiltration of pre-expanded foam or of pre-compressed foam occurs by a combination of capillary action and diffusion without swelling of the foam. Water induces swelling of the pre-compressed foam on a time scale of 1s, whereas glycerol swells the foam progressively over 10^5 s, after an initial incubation period of 10^3 s. When the foam is in the pre-expanded state, water and glycerol seep horizontally into the foam by capillary action; in contrast, water-rise and glycerol-rise in the vertical direction is initially by capillary action and then, once the Jurin height has been attained, diffusion leads to a much slower rate of seepage. Confirmation of the existence of a Jurin height for the vertical rise of water into pre-compressed foam or pre-expanded foam is obtained by X-ray computer tomography. Infiltration into pre-compressed foam by water or by glycerol involves the propagation of a swelling front, with liquid feeding first by capillary flow and then by diffusion within the cell walls. An understanding of liquid infiltration and the resultant swelling of foams is the first step in the design of actuating multi-scale lattices made from pre-compressed foam.

(keywords: foams, swelling, capillary rise, actuating lattice)

*Corresponding author at: Cambridge University Engineering Department, Trumpington St., Cambridge CB2 1PZ, UK
E-mail address: naf1@eng.cam.ac.uk (N.A. Fleck).

1. Introduction

Water seepage into a porous solid and subsequent swelling of the solid is ubiquitous in natural and artificial materials such as cellulose (wood, cotton), collagen-based leather and soils. A common manufacturing route for cellulose foams is to generate the foam in the wet state, and then to compress the foam and dry it in the compressed state. The dry foam has structural memory such that it re-swells when re-moistened. The re-swelling can be dramatic, for example a cellulose foam can swell by more than an order of magnitude when it is switched from the dry, compressed state to the wet, actuated state by the addition of water. The purpose of the present study is to gain insight into the relationship between the relative kinetics of fluid infiltration and of swelling. We shall focus on a cellulose foam in both the pre-compressed and pre-expanded states, and infiltrate the foams in the vertical and horizontal directions by ethanol, water and glycerol. Preliminary tests suggest that ethanol does not swell the foam whereas water and glycerol both expand the foam in one direction by a factor of about 15. Glycerol infiltrates the cellulose foam at a much slower rate than water, and also swells the foam over a much longer timescale.

The present study builds upon the recent observations of Mirzajanzadeh et al. (2019) on the seepage of water into a *pre-expanded* cellulose foam, absent swelling. Their experiments revealed that seepage is by a combination of (i) capillary action and (ii) diffusion in the presence of molecular traps within the cell walls of the cellulose. For the case of vertical rise of water into the foam, capillary rise initially dominates, and the height of the advancing wet front h scales with time t according to $h \propto t^{1/2}$. The so-called Jurin height is then reached at which point capillary forces are inadequate to lead to additional water-rise, and subsequent infiltration (at a reduced rate) is by diffusion within the cell walls. There is a significant experimental literature on these 2 distinct stages of the infiltration process, see for example Siddique et al. (2009), Kim et al. (2017), Ha et al. (2018) in addition to Mirzajanzadeh et al. (2019). Whilst all authors agree that capillary rise is the basis for the initial stage of infiltration there is no uniform agreement on the underlying physics of the second stage. Mirzajanzadeh et al. (2019) compared horizontal versus vertical water seepage in order to extricate the role of gravity, and employed x-ray computed tomography of the wet state in order to quantify the degree of infiltration in relation to surface observations of the wetting front.

The experimental results of the present study will be interpreted in terms of capillary flow within the cellular microstructure and diffusion within the cell walls. In order to introduce the fundamental notions of 1D capillary flow in a solid of inter-connected porosity we begin by

re-deriving the Washburn equation for the time-dependent capillary rise of a liquid in a vertical, circular cylindrical tube.

1.1 Capillary rise in a porous solid

A solid with sufficient porosity (typically more than 10%) can be treated as a network of interconnected channels; thus, liquid flow in a porous solid can be idealised by flow within a capillary tube. Upon neglecting inertial forces (Fries and Dreyer, 2008) and upon assuming a fixed contact angle between the liquid and the solid surfaces, liquid flow in a capillary tube is resisted by viscous drag in accordance with the Hagen-Poiseuille law. Consider a vertical capillary tube of uniform diameter *d*, brought into contact with liquid at its bottom end (see Fig. 1a). Liquid enters the tube as a result of suction on the liquid side of the meniscus, and consequently the height $h(t)$ of the liquid column increases with time *t*. Upon denoting the contact angle by ω, liquid-air surface tension by γ, liquid viscosity by η, liquid density by ρ and the acceleration due to gravity by *g*, the net pressure drop along the tube is of magnitude $(4\gamma\cos\omega/d)-\rho gh$ and this drives Poiseuille flow such that

$$\frac{4\gamma\cos\omega}{d}-\rho gh=\frac{32\eta h\dot{h}}{d^2} \tag{1}$$

with solution

$$h+\frac{4\gamma\cos\omega}{\rho gd}\ln\left[1-\frac{\rho gd}{4\gamma\cos\omega}h\right]=-\frac{\rho gd^2}{32\eta}t \tag{2}$$

as first given by Washburn (1921). As $t\to 0$, (2) reduces to

$$h=(\gamma d\cos\omega/4\eta)^{1/2}t^{1/2} \tag{3}$$

whereas as $t\to\infty$, $h(t)$ asymptotes to the limiting value of the Jurin height h_J (Jurin, 1717), where

$$h_J=\frac{4\gamma\cos\omega}{\rho gd}\,. \tag{4}$$

Note that (2) is also the solution to (1) in the absence of gravity, $g = 0$, and consequently (3) is the solution for horizontal capillary flow; for such horizontal flow, the Jurin height is unbounded, and capillary rise continues with increasing time, as sketched in Fig. 1b.

There have been a number of embellishments to the Washburn equation based on modifications to the assumed geometry. For example, Erickson & Park (2002) and Reyssat et al. (2008) considered tubes of circular cross-section but diverging along the flow direction, and

found that h no longer scaled with $t^{1/2}$. Shou et al. (2013) showed that capillary flow through the two-level heterogeneous porous architecture, made of different porosities at each level along the height, can also accelerate or decelerate the rise dynamics according to the heterogeneous arrangement of the porosity. Deviation from the Washburn law has also been observed in capillary rise of a liquid between flexible elastic sheets (Kim & Mahadevan, 2006; Aristoff et al., 2011; Cambau et al., 2011), in liquid rise within a swellable structure (Holmes et al., 2016), and in liquid rise between vertical wedges (Ponomarenko et al., 2011). Figliuzzi and Buie (2013) optimised the geometry of capillary channels to promote faster wicking than that of uniform cylinders. Gorce et al. (2016) discussed that horizontal liquid transport into a rigid power-law converging conical tube of shape defined by $a(x) = a_0\left(1 - x/L\right)^n$ and $n \geq 0$, where x is the coordinate along the tube axis, a is the radius of the tube, a_0 is the radius at the base location $x = 0$, and L is the tube length. Liquid flow in such tubes can only be faster than the constant radius capillary tube when $n < 5/3$, and the fastest liquid rise is achieved when $n = 5/6$. In contrast, liquid flow along an axisymmetric tube of increasing cross-sectional radius along the flow direction can be slower than that suggested by the Washburn law (Reyssat et al., 2008).

Models of fluid flow within deformable porous media were initially developed for the case of infinitismal deformation such as linear poroelasticity (see Biot (1972) and Coussy (2004)). More recently, models have been deveoped for finite deformation by Siddique et al. (2009). The forced infiltration of a fluid into porous media has been addressed by Sommer and Mortensen (1996), and the effect of large deformations of the solid skeleton upon flow of the interstitial fluid has been examined by MacMinn et al. (2016). However, little has been published on capillary flow in the presence of significant swelling of the porous solid.

Mirzajanzadeh et al. (2019) observed water-rise in their pre-expanded cellulose foam for liquid fronts beyond the Jurin height, and this subsequent phase is diffusion-controlled according to the following evidence. The observed scaling law of water-rise upon time, the insensitivity of water-rise to the direction of gravity, and the nature of the evolving density profile as measured by micro Computed Tomography (CT) each supports Fickian diffusion. Water diffusion occurs through the cellulose fibre network, along with trapping/de-trapping at molecular sites. The traps are sufficiently deep in terms of their enthalpy and are of sufficiently low concentration that the diffusion distance scales as $t^{1/2}$ in agreement with Fick's law, but the apparent diffusion constant is dependent upon the presence of traps in addition to the lattice diffusion constant. (Maps of diffusion regimes as a function of trap density and trap enthalpy have been generated recently by Raina et al. (2017)). Mirzajanzadeh et al. (2019) solved the

diffusion equations, and, upon comparing the predictions with the observed response, the diffusion constant and the ratio of trap density to lattice density were obtained. Lattice diffusion in the presence of deep molecular traps explains why the drying of a damp foam is a slow process: the emptying of water from traps requires diffusion through the adjacent lattice of low water content.

In summary, the primary transport mechanisms of liquid in a cellulose foam are capillary flow and diffusion. The main aim of the present study is to assess the role of swelling in such liquid transport by considering 3 fluids (water, ethanol and glycerol) that give rise to markedly different ratios of transport time to actuation time, and to a wide range of swelling strain. The sensitivity of the transport mechanism to the direction of swelling is also explored. The scope and outline of the study is as follows.

Scope and outline of study

Liquid migration in pre-expanded cellulose foam and in pre-compressed cellulose foam is measured by submerging one end of the foam specimen into a bath of water, glycerol or ethanol. High speed photography is used to record the rate of vertical and horizontal liquid rise and the associated swelling characteristics. The water content within the foam is determined by X-ray computed tomography, upon interruption of selected experiments on vertical water rise. A sequence of critical tests (A) to (F) are performed in order to make progressive deductions about the underlying mechanisms of the coupling between fluid migration into a foam and the attendant swelling. Each of these tests, and their objectives, are summarised as follows.

(A) Tests to determine the swelling response of pre-compressed cellulose, following rapid infiltration by water or glycerol. The degree of swelling is measured as a function of time for selected quantities of fluid uptake. It will be shown that the timescale for swelling of cellulose by water is on the order of 1 s whereas for glycerol the swelling time scale is on the order of 10^5 s. We shall show that the capillary rise time by water and by glycerol in *pre-expanded* cellulose foam are both on the order of 100 s and consequently the relative rates of foam-swelling and of capillary flow are markedly different for the two fluids. Thus, the cross-coupling between infiltration and swelling can be determined by performing infiltration tests on pre-compressed cellulose foam with either water or glycerol. This observation guides the remaining set of experiments.

(B) The reference case is considered in the form of a liquid that does not induce swelling of the foam: ethanol is chosen on this basis. Accordingly, the progressive infiltration of ethanol into pre-compressed and pre-expanded foam is measured. These experiments give insight into both capillary flow and diffusion into a foam in the pre-compressed and pre-expanded states without the added complexity of fluid-induced swelling.

(C) Dry pre-compressed cellulose is infiltrated by water (the case of rapid swelling), such that water-rise is in the vertical or horizontal directions, and swelling is transverse to the direction of water migration. By making suitable comparisons between the rate of infiltration by water in pre-compressed and pre-expanded foam, and by comparing with the infiltration of pre-expanded cellulose by ethanol, insight is obtained into the effect of swelling upon:

(i) capillary flow (horizontal flow and early vertical flow)

(ii) the Jurin height in vertical flow, and

(iii) diffusion beyond the Jurin height.

(D) Dry pre-compressed and dry pre-expanded cellulose are infiltrated by glycerol (the case of slow swelling), such that glycerol-rise is in the vertical or horizontal directions, and swelling is transverse to the direction of water migration. Swelling of pre-compressed foam by the presence of glycerol has a sufficiently large time delay that a separation of the wet front and the swelling front is observed.

(E) The 2D shape of the swelling front behind the seepage front is measured for vertical and horizontal water-rise and also vertical and horizontal glycerol rise, with the pre-compressed foam swelling in the transverse (horizontal) direction.

(F) The significance of constraint against vertical swelling during the vertical rise of water into pre-compressed foam is determined by applying a restraining pressure against vertical swelling. In additional tests on the vertical rise of water, a restraining displacement is imposed on the horizontal swelling of pre-compressed foam.

2. Test materials

Liquid rise experiments were performed on a cellulose foam[1] comprising a viscose cellulose matrix (dissolved cellulose of wood pulp) reinforced by cellulose fibres (Märtson et

[1] Supplied by Suvic Products Ltd., 3 Brunel Rd, Totton, Southampton SO40 3WX. http://www.suvic.co.uk/

al., 1999); this is the same batch of foam that was investigated previously by Mirzajanzadeh et al. (2019). Viscose cellulose fibres and sodium sulphate crystals were mixed mechanically and then heated to 90 – 95 °C; the sodium sulphate drains from the container leaving pore spaces, thereby generating a foam (Coda, 2005). This foam is termed 'pre-expanded' and has a density $\rho_f = 50$ kg m^{-3}; upon assuming that fully dense cellulose is of density $\rho_S = 1500$ kg m^{-3}, the relative density of the foam (in the dry state) is $\bar{\rho} = 0.03$. An alternative manufacturing route to make 'pre-compressed foam' involves compressing the foam after drainage of the sodium sulphate, and then drying the foam in the compressed state. The relative density of the pre-compressed cellulose foams (in the dry state) is $\bar{\rho} = 0.45$. The pre-compressed foams of thickness 2.4 mm have the potential to re-swell, depending upon the choice of added fluid. For example, the addition of water swells the foam by up to a factor of about 15 in the rise/thickness direction, giving a final thickness of $w_f \approx 35$ mm.

Scanning Electron Microscope (SEM) images of the dry pre-compressed cellulose foam are shown in Fig. 2a (plan view) and in Fig. 2c (side views). Magnified view of the micropores within the cell walls are included in the figures. Likewise, images of the dry pre-expanded cellulose foam are given in Figs. 2b (plan view) and 2d (side view). The relative length scale of the macropores (due to foaming) and the micropores (in the cell walls) are summarised in Fig. 2e. Typical optical images of the ingress of water into the pre-expanded foam are given in Fig. 2f. All tests were performed at room temperature (22 °C) using distilled water, ethanol and glycerol, for which salient properties are summarised in Table. 1.

We note from Table 1 that glycerol has a similar surface tension in air γ to that of water in air[2]. Likewise, glycerol has a similar density to that of water, but its viscosity is 3 orders of magnitude greater. This suggests that the Jurin height for vertical rise of glycerol into the cellulose foam is comparable to that of water but the rate of capillary flow will be much slower; recall the Washburn equations (2) and (3). In contrast, ethanol has a similar viscosity and a similar density to that of water, but its surface tension in air is less by a factor of approximately 3. Consequently, it is anticipated that it has a lower Jurin height (by a factor of approximately 3) for vertical rise in the cellulose foam than that of water, and a slower rate of capillary rise than that of water.

[2] The contact angles for the 3 fluids on this grade of cellulose are not known. Measurement of the contact angle is difficult since it absorbs fluids rapidly upon contact, rather than giving a stable droplet on the surface of the cellulose.

3. Swelling tests

An initial set of tests (category A as defined in the scope of study) were performed in order to measure the rate of swelling of the pre-compressed foam due to the rapid addition of water or glycerol; the addition of ethanol to a dry pre-compressed foam induced no detectable swelling. Dry pre-compressed cellulose foam samples of cross-sectional dimension 2 mm × 2 mm and initial thickness w_0 = 2.4 mm were immersed in a liquid reservoir on a time scale of 0.01s. The swelling/rise direction was horizontal, and the swelling stretch factor w / w_0 versus time t was measured by a high-speed camera and macro lens at a frame rate of 200 s^{-1} for the water test, and by a CMOS camera at a frame rate of 1 s^{-1} – 5 min^{-1} for the glycerol test, see Fig. 3a. The response curves were fitted by an empirical curve of the form $w / w_0 = 1 + \alpha \left[1 - \exp(-t / \tau) \right]$ in Fig. 3a, where $\alpha = 13.6$ for both water and glycerol, $\tau = 0.436$ s for water and $\tau = 1.4 \times 10^5$ s for glycerol.

In order to quantify the dependence of water-induced swelling upon water content, the foam was placed within a chamber of controlled humidity at room temperature. Dry pre-compressed foam samples of square cross-section 2 mm × 2 mm and thickness of w_0 = 2.4 mm were suspended inside a humidity chamber, at a relative humidity of 100% for selected time periods of 100s to 2500s. The final stretch factor w_∞ / w_0 (in the rise/swelling direction of the foam) and the water content of the foam m_w / m_f were measured, where m_w is the mass of the absorbed water and m_f is the mass of the dry foam. The response is summarised in Fig. 3b. For completeness, the specimens were dried for a period of 2000s by suspending them in laboratory air (at a temperature of 22 ^oC and relative humidity of 50%) and by measuring the residual stretch factor w_∞ / w_0: there is a small shrinkage by about 14%, as shown in Fig. 3b.

4. Liquid rise test methodology

4.1 Test Geometries

A wide range of possible types of liquid rise experiment can be performed, depending upon the choice of liquid, the infiltration direction of the liquid, the rise direction (that is, the swelling direction) of the foam, and whether the foam is in the pre-compressed or pre-expanded state.

Each experiment was initiated by bringing the bottom face of the foam into contact with a reservoir of liquid. The liquid level of the reservoir was maintained by the continued addition of liquid to the reservoir during each test. Each experiment is denoted by a sequence of three letters, as follows. A first letter V denotes fluid flow in '*Vertical*' direction; alternatively, a first

letter H denotes fluid flow in the '*Horizontal*' direction. A second letter V denotes that the rise/swelling direction of the foam is in the '*Vertical*' direction, whereas a second letter T denotes that the rise/swelling direction of the foam is in the '*Transverse*' direction. Finally, a third letter C denotes '*pre-compressed foam*', whereas a third letter E denotes '*pre-expanded foam*'. Thus, by way of example, VTE denotes *vertical* liquid rise in a pre-*expanded* foam where the rise/swelling direction of the foam is in the *transverse* (that is horizontal) direction, as shown in Fig. 4a. Three main experimental setups were employed for the pre-expanded foam (see Fig. 4) and for the pre-compressed foam samples (see Fig. 5), and the 3-letter nomenclature is adopted in the labelling of each type of test.

The liquid front height $h(t)$ is defined in Figs. 4 and 5 for each test type. A high-speed camera (frame rate in the range 25 – 200 s^{-1}) was used to record $h(t)$ when liquid migration was rapid, and a CMOS camera (frame rate in the range 0.5 – 2 min^{-1}) was used when liquid migration was slow.

4.2 Liquid rise in pre-expanded foam

In the VTE tests, dry foam samples of rectangular cross-section $v \times v$ (v = 22 mm) and length 200 mm were employed, unless otherwise stated. The liquid front height $h(t)$ was measured from the liquid level of the reservoir; see Fig. 4a. The foam specimens were located inside a transparent PMMA tube (of inner diameter 38 mm); the bottom end of the tube was placed inside the liquid reservoir and the top of the tube was covered by a plastic film containing a central hole of diameter 1 mm to minimize the effect of water and ethanol evaporation from the sample. The PMMA tube is not included in the sketch Fig. 4a for the sake of clarity.

In the VVE tests, dry foam samples were of rectangular cross-section $v \times v$ (v = 22 mm) and of length w_f = 30 mm (where w_f is the thickness of the dry pre-expanded foam in the rise/swelling direction). The liquid front height $h(t)$ was measured from the liquid level of the reservoir, see Fig. 4b.

The geometry of the specimen in the HTE tests is given in Fig. 4c: the specimens were of cross-section $v \times v$ and length 400 mm in the liquid-rise, X-direction. In these experiments, v equals 22 mm for water-infiltration, and v equals 11 mm for the ethanol-infiltration and for glycerol-infiltration[3]. The left-hand portion of the specimen was placed in the liquid reservoir while the weight of the right-hand portion was supported (not shown in sketch Fig. 4c.)

[3] The height v was chosen to be less than the Jurin height in each case. A small value of v was used for ethanol to minimize the error due to evaporation. For glycerol, infiltration is slow and so a small value of v allows for a more rapid test.

Measurement of the liquid-front migration was initiated when the liquid front reached the step in geometry (i.e. at $X = 0$) along the trajectory shown in Fig. 4c. The time for the liquid front to migrate from the reservoir to $X = 0$, and the associated trajectory length, were added to the measured time and liquid front length, respectively.

4.3 Liquid rise in pre-compressed foam

The test setup in the liquid rise tests on the pre-compressed foams is the same as that employed on the pre-expanded foams. The dimensions of the specimens are as follows. In the VTC tests, dry foam samples were of rectangular cross-section $v \times w_0$ (where $v = 22$ mm and w_0 is the thickness of the dry pre-expanded foam in rise/swelling direction) and of length 200 mm, unless otherwise stated. The geometry of the VTC test at t=0 and at an intermediate time are shown in the sketch of Fig. 5a.

In the VVC tests, dry pre-compressed foam samples were of rectangular cross-section $v \times v$ ($v = 22$ mm) and of length $w_0 = 2.4$ mm, where w_0 is the thickness of the dry pre-compressed foam in the rise/swelling direction. Again, sketches are given of the initial state and of an intermediate state, see Fig. 5b. In Fig. 5b, $H(t)$ is the backward map of the liquid front height $h(t)$ from the current, deformed configuration to the reference, undeformed configuration.

The geometry of the specimen in the HTC tests is given in Fig. 5c, both at the start of the test ($t = 0$) and at an intermediate time $t > 0$. The specimens had an initial cross-section of $v \times w_0$ (where $w_0 = 2.4$ mm is the initial thickness of the dry pre-compressed foam) and length of 400 mm in the liquid-rise, X-direction. In these experiments, $v = 22$ mm for the water-infiltration tests and $v = 11$ mm for the ethanol-infiltration and glycerol-infiltration tests.

5. Measurement of liquid infiltration

5.1 Test Series B: ethanol-infiltration of pre-compressed and pre-expanded foam

The measured wet front height h versus time t for the ethanol-rise tests for all test configurations are shown in Fig. 6a, with the following background of interpretation. We emphasise that the ethanol neither swells the pre-compressed foam nor the pre-expanded foam. Assume that the initial migration of ethanol into the foam is due to capillary action, and recall that ethanol induces negligible swelling of the foam. Recall that the Washburn relations (2) and (3) are relevant for vertical flow, such that gravity opposes liquid rise, whereas for horizontal flow the value of gravitational acceleration g vanishes, and (3) applies for all time,

t. Since ethanol does not swell the foam, the difference in response between the pre-expanded and the pre-compressed foams is due to the difference in capillary size: the Washburn equations (2) and (3) suggest that capillaries of larger diameter (as in the pre-expanded state) lead to faster liquid rise.

Ethanol is drawn horizontally into the pre-expanded foam at a faster rate than the pre-compressed foam due to the larger capillaries in the pre-expanded state, compare the responses for ethanol-rise in the HTE with HTC configurations. The height scales with time according to $h \propto t^{1/2}$ for both geometries, as anticipated by (3), with a shift to longer times for the pre-compressed foam. Now compare the responses for *horizontal* ethanol flow in the HTC geometry and for *vertical* ethanol flow in the VTC configuration. It is found that the $h(t)$ response is almost identical for the VTC and HTC orientations, with the interpretation that the capillaries in these pre-compressed samples are sufficiently narrow for the rate of ethanol-rise to be unaffected by the direction of gravity. Also, the Jurin height for the VTC much exceeds the maximum height achieved over the duration of the VTC test[4]. In contrast, the capillaries in the pre-expanded foam are sufficiently wide for the Jurin height $h_J \approx 20$ mm to be achieved within the vertical flow experiment VTE. The foam is almost isotropic in the pre-expanded state such that the $h(t)$ response for vertical rise of the ethanol is almost the same when the direction of *pre-expansion* of the foam is in the vertical direction (VVE test) or in the horizontal direction (VTE test).

The role of inertia in ethanol-rise can be assessed as follows. There is a short initial period of duration $t^* = \rho d^2 / (32\eta)$ for which inertia dominates the flow, as discussed by Fries and Dreyer (2008) and by de Gennes et al. (2013). The effective value of *d* for the pre-expanded foam can be estimated from the Jurin height and could be on the order of 1mm, consistent with Fig. 2. This implies a duration of approximately $t^* = 25$ms. Upon recalling that the cell size for the pre-compressed foam is 1 order of magnitude less than that of the pre-expanded foam, we conclude that t^* is on the order of 0.25 ms for this state of foam. The initial period of inertia-dominated flow is below the time resolution of the experiments reported herein, and does not influence the observed scaling laws of fluid rise versus time. This conclusion holds for all 3 fluids of the present study.

[4] Continuation of the tests for a longer period is problematic due to evaporation of the ethanol.

5.2 Test Series C: water migration into pre-compressed foam

The rate of infiltration by water into pre-compressed foam is now reported, and compared with the previous results for water migration into pre-expanded foam, as taken from Mirzajanzadeh et al. (2019). Recall from Fig. 3 that the addition of water to pre-compressed foam induces rapid swelling.

The measured wet front height h versus time t for the water-rise test for all configurations is shown in Fig. 6b. We first review the results for the pre-expanded foam. The VTE test (vertical water rise) reveals two stages of water migration: stage I in support of the classical Washburn law (3), such that $h \propto t^{1/2}$ for the initial 10 seconds, then after the Jurin height h_J has been attained, there follows a slower rate of diffusion within the cell walls (for $h > h_J \approx 24\,\text{mm}$). In contrast, the HTE test reveals that, in the absence of gravity, the rate of water-rise throughout the test follows the same power law, $h \propto t^{1/2}$, as that observed in the initial phase of stage I of the VTE test. This is consistent with the prediction (3) of the Washburn law absent gravity, $g \to 0$. The responses in the VVE and VTE tests are almost identical, indicating that the pre-expanded foam is almost isotropic in response, as already deduced from ethanol-infiltration of the VVE and VTE geometries, recall Fig. 6a.

Now consider water migration within the dry pre-compressed foam and the significance of the severe lateral swelling (by an order of magnitude) in a direction transverse to that of water infiltration. The VTC test again reveals two stages of water-rise but the behaviour is different to that of the corresponding test VTE on the pre-expanded foam: now, stage I is characterised by $h \propto t^{0.73}$ which does *not* support the Washburn law. We interpret the change in power law from 0.5 to 0.73 as evidence of active pumping of the water in the expanding capillaries of the pre-compressed foam, and we shall generate a simple model for this in a subsequent section. An apparent Jurin height is attained at $h_J \approx 80$ mm, with subsequent slow migration of water by diffusion within the cell walls of the foam. (Later, we shall detail the water content profile in the foam as additional evidence for the existence of the apparent Jurin height at $h_J = 80$ mm.) The diffusion response in the VTC test converges to that of the VTE test, with the interpretation that water diffusion occurs at a similar rate within the pre-compressed and pre-expanded cell walls.

The HTC test reveals that, in the absence of gravity, the rate of water migration follows the same power law, $h \propto t^{0.73}$, as that observed in stage I of the vertical-rise test, specimen VTC.

However, the absence of gravity in resisting water flow by capillary action implies that the Jurin height is now unbounded and the power law $h \propto t^{0.73}$ is maintained throughout the duration of the test. The case of vertical water-rise in a pre-compressed foam with the rise/swelling direction also vertical, case VVE, is included in Fig. 6b. Recall that the initial thickness of the pre-compressed foam is $w_0 = 2.4$ mm and so the maximum height of water-rise of 30mm corresponds to the height of the foam upon full swelling. The rate of water-rise in this test is now faster than that of the HTC and the test terminates before the Jurin height has been attained.

5.3 Test Series D: glycerol migration into pre-expanded and pre-compressed foam

Consider first the case of glycerol migration within the pre-expanded foam, see Fig. 6c. In broad terms, the response is similar to that water and ethanol infiltration: initially, the Washburn regime of capillary rise is observed for the case of vertical rise of the glycerol in the VTE and VVE tests, followed by diffusion within the cell walls once the Jurin height $h_J \approx$ 18 mm has been attained. The rate of initial migration by glycerol is slower than that of water and ethanol, consistent with the fact that it has a higher viscosity but comparable densities and surface tensions, as noted in Table 1. Furthermore, the HTE test reveals that, in the absence of gravity, the rate of glycerol migration throughout the test follows $h \propto t^{1/2}$ in accordance with the Washburn law (3). The overlap of the VVE response with that of the VTE result again confirms that the foam behaves in an isotropic manner in the expanded state.

Second, consider glycerol migration within the pre-compressed foam, as reported in Fig. 6c. In order to aid interpretation of the results, recall from Fig. 3 that swelling of the foam occurs after an incubation period of approximately 10^3 s. (In contrast, the incubation period for water-induced swelling is on the order of 10^{-2} s.) Consequently, it is anticipated that initial capillary rise in the VTC tests will occur before swelling of the foam can occur, and thereby resemble the infiltration of ethanol into the pre-compressed foam in the corresponding VTC tests as reported in Fig. 6a. It is noted form Fig. 6c that glycerol-rise in the VTC test reveals three regimes, as follows. Stage I (part I) supports the Washburn law for the initial 10^3 s. The dependence of h upon t changes to a power law of the form $h \propto t^{0.73}$ in stage I (part II), which resembles that observed in stage I water-rise in the VTC tests. The Jurin height is attained at $h_J \approx$ 80 mm, and subsequently liquid rise is much slower in the final stage II of diffusion-controlled infiltration. The HTC test reveals that in the absence of gravity, the rate of glycerol-rise throughout the test follows the same scaling law $h \propto t^{0.73}$ as that observed in the

intermediate regime of the VTC test. This is again suggestive of capillary rise absent gravity, $g \to 0$. The liquid rise test results for all the ethanol, water and glycerol infiltration are summarised in Table 2.

6. The 2D evolution of wetting and swelling fronts: test series E

Horizontal water migration in pre-compressed foam in the HTC test reveals that, in the absence of gravity, the rate of water infiltration follows the same power law, $h \propto t^{0.73}$, as that observed in the initial phase of stage I of the VTC test. This suggests that, for the VTC test, the early regime of vertical liquid rise in the pre-compressed foam is due to capillary rise, and the knee point in the plot denotes the Jurin height h_J. We proceed to provide additional evidence for the existence of the Jurin height in the VTC tests by measuring the water content profile in the foam via CT scans, and also seek to explain the observed capillary rise rate of $h \propto t^{0.73}$ by analysing the swelling profile of the pre-compressed foam during water and glycerol infiltration in the VTC and HTC tests.

6.1 Water content profile

The spatial distribution of volume fraction of water in the foam was measured by micro computed tomography (CT) after interruption of a vertical water-rise test on the pre-expanded foam, VTE, and on the pre-compressed foam, VTC. Checks were made on the accuracy of the CT measurements by performing additional destructive tests following the VTE test, whereby the specimen was cut into transverse slices and the density of each slice was measured via its weight and volume. The computed tomography X-ray scans were performed using a 50 kV X-ray source, a 1s exposure time and a spatial resolution of 36 μm per voxel unit: this is the highest achievable resolution as dictated by the dimension of the foam specimens and the performance of the CT machine[5].

Each scan of the foam samples takes about one hour, and, in order to prevent migration of water along the foam specimen during the measurement, the foam samples were frozen at the desired instant during the test, and maintained in the frozen state during the CT scan. The procedure was as follows. When the wet front attained the desired position in the vertical water-rise test, the foam sample was removed quickly from the water reservoir and immersed in liquid nitrogen. Infiltration of the foam by liquid nitrogen was prevented by sheathing the foam in a

[5] Nikon X-TEK (XT H 225ST) machine.

thin film of low density polyethylene (LDPE) immediately prior to immersion. The foam was maintained in the frozen state during the CT scan by suspending it above a bath of liquid nitrogen during the CT scans: the temperature of the foam was maintained below – 70 °C by this arrangement. In order for the foam samples to fit inside the CT machine (and maximise the resolution), the samples were cut into pieces of length 45 mm after freezing. The volume fraction of water was measured in slices of thickness 1mm (along the height of the foam column) by post-processing CT software[6] following calibration of the CT scan results against the density of distilled water, that is 1000 kg m^{-3}. The average volume fraction of the water F_w within each slice in the current configuration is calculated from a calibrated density histogram of each slice. We convert F_w in the current configuration to a water volume fraction in the fully expanded state of the foam using $f_w = F_w w(Z,t) / w_f$, where $w(Z,t)$ is the current width of the foam, and w_f is the fully expanded thickness of the foam for the case of full water saturation, recall Fig. 3b. This scaling allows us to compare directly the water content in the VTE and VTC test configurations, as reported below.

6.2 Results and discussion for the water content profiles

A representative CT image of the cellulose foam in the VTC test in Fig. 7a shows the distribution of water at mid-plane of the foam at t = 60 s. The spatial distributions of the volume fraction of the water f_w in the VTC test, at t = 60 s and t = 900 s, are compared with that of the VTE test at t = 2000 s in Fig. 7b. We emphasize that f_w is the calculated water volume fraction if the foam were in the fully expanded configuration. It was shown in Fig. 5 of Mirzajanzadeh et al. (2019) that, within stage I of water-rise in VTE tests, the volume fraction of water as a function of height asymptotes to a steady state. This suggests that the foam microstructure behaves as an ensemble of capillary tubes of varying diameter (Mirzajanzadeh et al., 2019). A comparison of the three distributions of volume fraction of water in Fig. 7b reveals the following:

(i) The foam retains substantially more water if it is initially in the pre-compressed state than in the pre-expanded state.

(ii) The water content in the VTC test for Z > 20 mm (i.e. above the Jurin height of the pre-expanded foam) decreases with increasing time. This shows that the water drains from the

[6] Post-processing analysis of the reconstructed CT images was performed using VGStudio MAX 2.2 software.

foam after it swells, and the concentration profiles of the pre-expanded and pre-compressed foams converge with increasing time.

6.3 Swelling-induced shape profiles in the VTC and HTC tests

Additional insight into the regime of enhanced liquid infiltration, such that $h \propto t^{0.73}$ in stage I capillary rise of water and of glycerol in the VTC and HTC tests, is obtained by analysing the shape of the swelling profiles of the pre-compressed foam as follows. Consider first water infiltration of the pre-compressed foam. A sample image of a pre-compressed foam during a VTC test is shown in Fig. 8a, along with the measured shape profiles plotted on a logarithmic scale in Fig. 8b. Measured swelling profiles for the water-rise in the VTC and HTC tests are given in Fig. 8c. The swelling profiles of the pre-compressed foam in Fig. 8c reveal that the width 2*b* of the foam at a distance ζ behind the wet front remains almost uniform during water-rise in the VTC and HTC tests. The profile immediately behind the wet front in Fig. 8b can be fitted by the expression $b(\zeta) = k\left(\zeta / \zeta_0\right)^n + b_0$ where k = 3mm, ζ_0=1mm, n = 0.46, and $2b_0$ = w_0 = 2.4 mm. This curve-fit is included in Fig. 8c as solid red lines.

Sequential images of glycerol-rise in the VTC and HTC tests are shown in Fig. 9a, and the shape of the profile is plotted on a logarithmic scale in Fig. 9b. Again, the swelling zone behind the front asymptotes to a constant shape. The measured swelling profiles in the proximity of the wet front in the HTC test can be fitted by curve $b(\zeta) = k\left(\zeta / \zeta_0\right)^n + b_0$ where k = 1.3 mm, ζ_0=1mm, n = 0.55, and $2b_0$ = w_0 = 2.4 mm which is included in plot Fig. 9b as solid red lines.

6.4 A simple model of capillary pumping

The swelling zone in the HTC experiments for horizontal water and glycerol infiltration into pre-compressed foam quickly settles down to a constant shape. This allows for a simplification of the analysis as follows. Idealise a representative capillary tube within the foam (in the post-swollen state) by a circular cylinder of radius a_2 and length h, with the axis of symmetry of the cylinder along the horizontal direction, see Fig. 10. Assume that, upstream, the foam is dry and in the pre-compressed state, and the same capillary exists as a long circular cylinder of radius $a_1 < a_2$, with a transition zone linking the two cylinders. The transition zone has the shape of a truncated cone. Water, or glycerol, migrates along the axis of the expanded

zone (capillary tube of radius a_2 and the transition zone) with a relative velocity $\dot{h}$ and this gives rise to a pressure drop of Δp_2 over the length *h*. The assumption of Poiseuille flow inside the capillary demands that

$$\Delta p_2 = \frac{8\eta h}{a_2^{\,2}}\dot{h}\,. \tag{5}$$

Additionally, a pressure drop Δp_1 exists within the transition zone of progressively swelling foam. Assuming that this pressure drop is due to viscous loss, dimensional analysis demands that

$$\Delta p_1 = \frac{\beta\eta}{a_1}\dot{h} \tag{6}$$

in terms of a geometrical shape factor β that is a function of the shape of the non-evolving transition zone. Now equate the net pressure drop $\left(\Delta p_1 + \Delta p_2\right)$ to the sum of the capillary pressure $2\gamma / a_1$ and to a constant actuation pressure Δp_a associated with self-inflation of the foam after wetting to give

$$\Delta p_1 + \Delta p_2 = \frac{\beta\eta}{a_1}\dot{h} + \frac{8\eta h}{a_2^{\,2}}\dot{h} = \frac{2\gamma}{a_1} + \Delta p_a \quad . \tag{7}$$

Integration of (7) leads directly to the result

$$\frac{\beta\eta h}{a_1} + \frac{4\eta h^2}{a_2^{\,2}} = \left(\frac{2\gamma}{a_1} + \Delta p_a\right)t + C \tag{8}$$

in terms of a constant *C* that can be interpreted as the time to establish the steady state swelling zone. We note from (8) that the rate of liquid ingress $\dot{h}$ scales with time *t* at a rate that is intermediate between linear scaling, $h \propto t$ and a square-root law, $h \propto t^{1/2}$. The observed dependence in Figs. 6b and 6c is $h \propto t^{0.73}$. Note also that the mechanical pumping contribution Δp_a increases the rate of liquid infiltration but does not change the functional dependence of *h* upon *t*.

7. Restrained seepage: test series F

Preliminary experiments reveal that the surface wetting of a dry, pre-compressed cellulose plate by an isolated water droplet leads to the formation of a surface blister. In such an example, the blister is constrained by surrounding dry foam in the stiff, unswollen state. The

significance of constraint against swelling from vertical rise of water into pre-compressed foam is now assessed.

7.1 Water-rise in a restricted swelling foam

The effect of constraint against swelling of the foam due to water infiltration was measured via two experiments, one to explore the significance of vertical constraint against vertical swelling, and the other to explore lateral constraint against lateral swelling. The first test employed the VVC arrangement (with v = 22 mm, and w_0 = 2.4 mm as defined in Fig. 5b); a restraining pressure p_0 was imposed against expansion/swelling (see the inset in Fig. 11a) by placing dead weights on top of the pre-compressed foam. In order for this load to be supported at the immersed, bottom end of the foam, a thin steel mesh plate was used to support the bottom face of the foam column. The second experiment was of VTC type (with v = 40 mm and w_0 = 2.4 mm, see Fig. 5a). Lateral swelling of the foam in the transverse direction is prevented by the presence of glass sheets of thickness 5mm, see Fig. 12b.

7.2 Results for constrained swelling

The first set of these experiments involved the application of selected values of restraining pressure p_0 in the range of 0 to 9.2 kPa in the VVC tests. The water front height h (as measured in the deformed configuration) within the foam is plotted as a function of time t in Fig. 11a. In all tests, the time for the water to rise to the top of the pre-compressed foam is 3s; this is comparable to the foam swelling time of 1s, recall Fig. 3a. Thus, there is coupling between capillary flow and swelling of the foam. As a consequence, the rate of water-rise exceeds the Washburn scaling of $h \propto t^{1/2}$, and approaches linear scaling $h \propto t$ at low confining pressures (less than 1 kPa). The plateau in water-rise is due to the fact that the foam column is wet over its full height after 3s, rather than the attainment of the Jurin height. It is instructive to re-plot the data shown in Fig. 11a as the wet front height in the *un-deformed* configuration (Lagrangian coordinate system) in the form of $H(t)$ versus time t (see Fig. 5b) as shown in Fig. 11b. We note that the water-rise height in the VVC test in the un-deformed configuration of the foam lies on a unique curve which follows Washburn law, regardless of the superimposed confining pressure. We conclude that the sensitivity of $h(t)$ in the deformed configuration to pressure p_0 is due to the low strength of the foam in the wet, swollen state.

The second test is of VTC geometry but fully constrained against swelling of the foam in the transverse (lateral) direction, see Fig. 12. The wet front height h vs time t for the aforementioned test is compared with the original VTC and VTE tests in Fig. 12a. Constraint against swelling leads to much slower water rise, and the Washburn law is recovered with a water-rise characteristic of $h \propto t^{1/2}$. It is instructive to compare this response with that of ethanol-rise in the VTC test, and to achieve this the relevant data from Fig. 6a are replotted in Fig. 12a. Recall that ethanol does not swell the pre-compressed foam. The responses are similar with a slightly faster rate of ethanol than water.

9. Concluding remarks

The effect of fluid-induced swelling upon the infiltration of a liquid into a pre-compressed cellulose foam has been explored. Water and glycerol induce substantial one-dimensional swelling by 15 times the original thickness, whereas ethanol does not swell the foam. The time required for swelling and the capillary (Jurin) rise time are summarised in Table 3 for each fluid: the relative time for swelling versus fluid rise differs significantly for the 3 fluids. Experiments suggest two regimes of liquid-migration in the vertical direction for a pre-expanded foam under the influence of gravity. Initially, transport is driven by capillary forces but this mechanism becomes non-operative above the so-called Jurin height of 24 mm, 20 mm and 18 mm for water, ethanol and glycerol, respectively. Water continues to rise above the Jurin height, albeit at a slower rate, driven by diffusion along with by trapping at deep traps (i.e. sites within the foam that have a high affinity for the liquid) as discussed by Mirzajanzadeh et al. (2019). The transport of water in a horizontal pre-expanded foam (where gravity plays no role) is always dominated by the fast capillary mechanism.

In the presence of lateral swelling of the pre-compressed foam during liquid flow in the vertical or horizontal directions, liquid migration deviates from the Washburn law such that the liquid front length h scales with time t according to $h \propto t^{0.73}$. This change in scaling law is due to the fact that the capillary pressure is set by the small size of the cellulose cells in the pre-compressed state, yet liquid migration is through the expanded foam in the swollen state. Mechanical pumping may also be involved, and the model developed herein suggests that pumping gives a similar qualitative effect to that of surface tension: it is not possible to delineate between surface tension-driven liquid-rise and mechanical pumping. Further work is needed in order to understand the precise nature of these scaling laws.

Acknowledgements

The authors are grateful for financial support of this work in the form of an ERC MULTILAT grant 669764.

References

Aristoff, J. M., Duprat, C. & Stone, H. A., 2011. Elastocapillary imbibition. *International Journal of Non-Linear Mechanics,* 46(4), pp. 648-656.

Biot, M. A., 1972. Theory of finite deformations of porous solids. *Indiana University Mathematics Journal,* 21(7), pp. 597-620.

Cambau, T., Bico, J. & Reyssat, E., 2011. Capillary rise between flexible walls. *EPL (Europhysics Letters),* 96(2), p. 24001.

Coda, R., 2005. *a study of cellulose based biodegradable foams and sponges,* s.l.: M.S. thesis, Georgia Institute of Technology.

Coussy, O., 2004. *Poromechanics.* s.l.:John Wiley & Sons.

De Gennes, P.G., Brochard-Wyart, F. & Quéré, D., 2013. *Capillarity and wetting phenomena: drops, bubbles, pearls, waves*. Springer Science & Business Media.

Erickson, D. D. L. & Park, C. B., 2002. Numerical simulations of capillary-driven flows in nonuniform cross-sectional capillaries. *Journal of colloid and interface science,* 250(2), pp. 422-430.

Figliuzzi, B. & Buie, C. R., 2013. Rise in optimized capillary channels. *Journal of Fluid Mechanics,* Volume 731, pp. 142-161.

Fries, N. & Dreyer M., 2008. The transition from inertial to viscous flow in capillary rise. *Journal of colloid and interface science,* 327(1), pp. 125-128.

Gorce, J.-B., Hewitt, I. J. & Vella, D., 2016. Capillary imbibition into converging tubes: Beating washburn's law and the optimal imbibition of liquids. *Langmuir,* 32(6), pp. 1560-1567.

Holmes, D. P., Brun, P.-T., Pandey, A. & Protière, S., 2016. Rising beyond elastocapillarity. *Soft matter,* 12(22), pp. 4886-4890.

Jurin, J., 1717. An Account of Some Experiments Shown before the Royal Society; With an Enquiry into the Cause of the Ascent and Suspension of Water in Capillary Tubes. *Philosophical Transactions,* 30(351-363), pp. 739-747.

Kim, H.-Y. & Mahadevan, L., 2006. Capillary rise between elastic sheets. *Journal of Fluid mechanics,* Volume 548, pp. 141-150.

Kim, J., Ha, J. & Kim, H.-Y., 2017. Capillary rise of non-aqueous liquids in cellulose sponges. *Journal of Fluid Mechanics,* Volume 818.

MacMinn, C. W., Dufresne, E. R. & Wettlaufer, J. S., 2016. Large deformations of a soft porous material. *Physical Review Applied,* 5(4), p. 044020.

Märtson, M. et al., 1999. Is cellulose sponge degradable or stable as implantation material? An in vivo subcutaneous study in the rat. *Biomaterials,* 20(21), pp. 1989-1995.

Mirzajanzadeh, M., Deshpande, V. S., Fleck, N. A., 2019. Water Rise in A Cellulose Foam: by Capillary or Diffusional Flow? *J. Mech. Phys. Solids*, **124**, pp. 206-219. https://doi.org/10.1016/j.jmps.2018.10.009

Raina, A., Deshpande, V. S. & Fleck, N. A., 2017. Analysis of electro-permeation of hydrogen in metallic alloys. *Phil. Trans. R. Soc. A,* 375(2098), p. 20160409.

Ponomarenko, A., Quéré, D. & Clanet, C., 2011. A universal law for capillary rise in corners. *Journal of Fluid Mechanics,* Volume 666, pp. 146-154.

Reyssat, M., Courbin, L., Reyssat, E. & Stone, H. A., 2008. Imbibition in geometries with axial variations. *Journal of Fluid Mechanics,* Volume 615, pp. 335-344.

Shou, D., Ye, L., Fan, J. & Fu, K., 2013. Optimal design of porous structures for the fastest liquid absorption. *Langmuir,* 30(1), pp. 149-155.

Siddique, J. I., Anderson, D. M. & Bondarev, A., 2009. Capillary rise of a liquid into a deformable porous material. *Physics of Fluids,* 21(1), p. 013106.

Sommer, J. L. & Mortensen, A., 1996. Forced unidirectional infiltration of deformable porous media. *Journal of fluid mechanics,* Volume 311, pp. 193-217.

Washburn, E. W., 1921. The dynamics of capillary flow. *Physical review,* 17(3), p. 273.

Table 1. Liquid properties at 22 ºC.

liquids	γ (N m^{-1})	η (Pa s)	ρ (kg m^{-3})
water	0.072	0.9×10^{-3}	1000
ethanol	0.022	1.074×10^{-3}	789
glycerol	0.063	1.178	1261

Table 2. Behaviour of the liquid rise in the cellulose foam for the different tests.

liquids	liquid rise tests	stage I	stage II
water, ethanol and glycerol	VTE	$h \sim t^{1/2}$	$h' \sim t'^{1/2}$
	HTE	$h \sim t^{1/2}$	not observed
	VVE	$h \sim t^{1/2}$	$h' \sim t'^{1/2}$
water	VTC	$h \sim t^{8/11}$	$h' \sim t'^{1/2}$
	HTC	$h \sim t^{8/11}$	not observed
	VVC	$h \sim t$	-
glycerol	VTC	$h \sim t^{1/2}$ and $h \sim t^{8/11}$	$h' \sim t'^{1/2}$
	HTC	$h \sim t^{8/11}$	not observed
ethanol	VTC	$h \sim t^{1/2}$	not observed
	HTC	$h \sim t^{1/2}$	not observed

Note. Assume that the second regime of water-rise initiates when the Jurin height is attained. Accordingly, in stage II, rescale $h(t)$ to $h'(t')$ where $h' \equiv h - h_J$ and $t' \equiv t - t_J$, where t_J is the time to attain the point of inflection on the $h(t)$ curve, that is, the time to attain the Jurin height h_J.

Table 3. Swelling and capillary rise time for the used fluids.

liquids	swelling time in *pre-compressed* foam (s)	capillary rise time in *pre-expanded* foam (s)
water	1	10
ethanol	*no swelling occurs*	8
glycerol	4×10^{5}	100

FIGURE CAPTIONS

Fig. 1. (a) Sketch of capillary rise in a vertical tube; (b) Sketch of the capillary rise height versus time in the presence of gravity as given by equation (2), in the absence of gravity via equation (3), and the *observed* behaviour. The equilibrium height in the vertical capillary tube, in the presence of gravity, is the Jurin height h_J.

Fig. 2. (a) SEM image of the dry pre-compressed foam with the Rise/swelling Direction of the foam RD perpendicular to the page; (b) SEM image of the dry pre-expanded foam with RD perpendicular to the page; (c) SEM image of the dry pre-compressed foam with RD as shown; (d) SEM image of the dry pre-expanded foam with RD as shown; (e) Schematic of the two scales of the porosity in pre-expanded foam; (f) Optical image of the dry and partially wet pre-expanded cellulose foam.

Fig. 3. (a) Measured swelling stretch factor w/w_0 with time t for the immersion of the pre-compressed foam in water and glycerol, where w is the time-dependent thickness of the foam in the rise/swelling direction and w_0 = 2.4 mm is the initial thickness of the foam in rise/swelling direction. The solid lines show the fitted curve $w/w_0 = 1 + \alpha\left[1 - \exp(-t/\tau)\right]$, where α = 13.6 and τ = 0.436 s for water and $\tau = 1.4 \times 10^5$ s for glycerol. (b) Measured swelling stretch factor w_∞ / w_0 at long time versus water content m_w / m_f. The measured normalized swelling factor upon drying is shown as filled symbols.

Fig. 4. (a) Test geometry for the vertical reservoir-fed test with the Rise/swelling Direction RD of the foam in transverse direction for the pre-expanded foam (VTE); (b) Test geometry for the vertical reservoir-fed test with the RD in the flow direction for the pre-expanded foam (VVE); (c) Test geometry for the horizontal reservoir-fed test with the RD in the transverse direction for the pre-expanded foam (HTE).

Fig. 5. (a) Test geometry for the vertical reservoir-fed test with the Rise/swelling Direction RD of the foam in transverse direction for the pre-compressed foam (VTC); (b) Test geometry for the vertical reservoir-fed test with the RD in the flow direction for the pre-compressed foam (VVC); (c) Test geometry for the horizontal reservoir-fed test with the RD in the transverse direction for the pre-compressed foam (HTC).

Fig. 6. Measured liquid front length h versus time t for the pre-compressed and pre-expanded foams for different test arrangements with respect to the flow direction and the rise/swelling direction RD of the foam using (a) ethanol, (b) water and (c) glycerol.

Fig. 7. (a) The 3D reconstructed computed tomography X-ray image of the pre-compressed cellulose foam during the VTC water reservoir-fed test at $t = 60$ s; (b) Measured volume fraction of water f_w in the VTC test versus position Z at time $t = 60$ s and $t = 900$ s compared with the volume faction of water f_w profile in the VTE test at time $t = 2000$ s.

Fig. 8. (a) Image of the pre-compressed foam upon water rise in the VTC test; (b) Measured swelling profiles of the foam versus coordinate ζ during the water rise in the VTC test at selected times: red solid line shows the fitted curve $b(\zeta) = k\left(\zeta / \zeta_0\right)^n + b_0$ with $k = 3$mm, $\zeta_0 = 1$ mm, $n = 0.46$, and $2b_0 = w_0 = 2.4$ mm; (c) Measured swelling profiles of the pre-compressed foam for the water rise in the VTC and HTC tests at selected times.

Fig. 9. (a) Sequential images of the pre-compressed foam during the glycerol rise in the VTC test; (b) Measured swelling profile of the pre-compressed foam in glycerol rise in the VTC and HTC tests at selected times.

Fig. 10. Sketch of horizontal capillary flow in a swelling tube.

Fig. 11. (a) Measured water front height h versus time t in the constrained VVC tests for selected values of compressive pressure p_0. (b) Wet front height in the un-deformed configuration of the foam H versus time t in the constrained VVC tests (see Fig. 5b).

Fig. 12. (a) Measured wet front height h with time t for the VTE, VTC and swelling confined VTC reservoir-fed tests; (b) A sketch of the VTE, swelling-free VTC and swelling-confined VTC reservoir-fed tests.

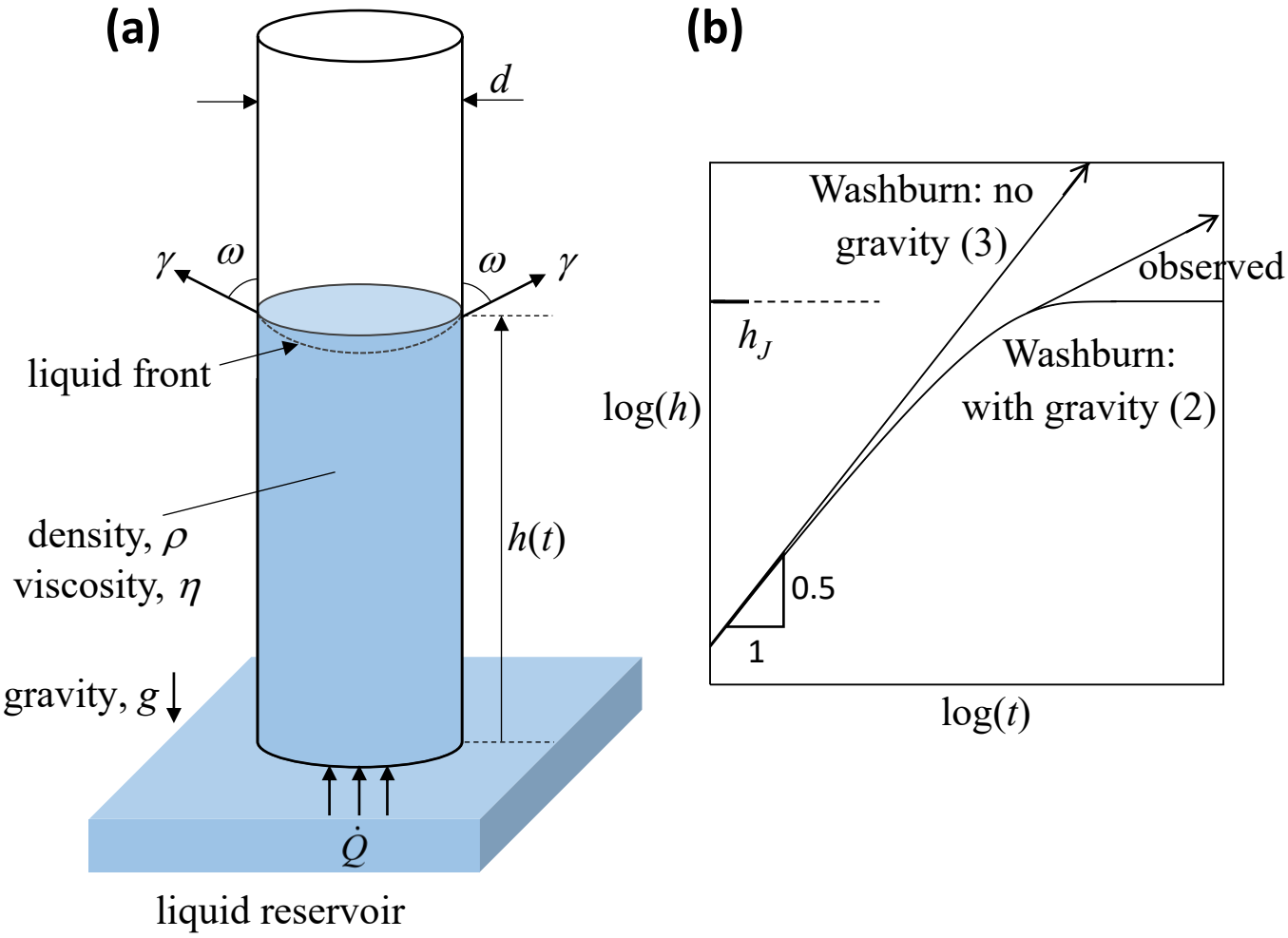

Fig. 1. (a) Sketch of capillary rise in a vertical tube; (b) Sketch of the capillary rise height versus time in the presence of gravity as given by equation (2), in the absence of gravity via equation (3), and the *observed* behaviour. The equilibrium height in the vertical capillary tube, in the presence of gravity, is the Jurin height h_J.

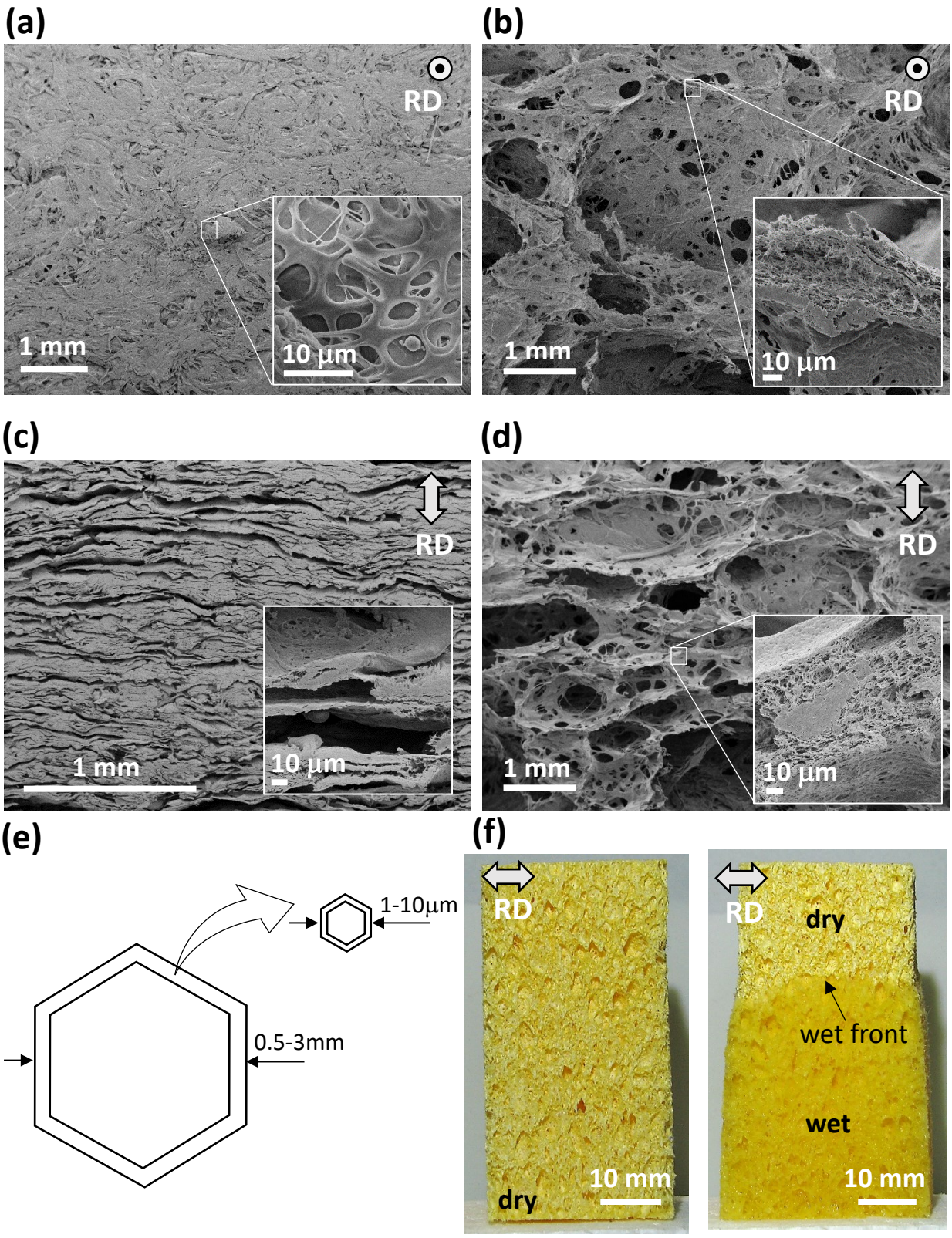

Fig. 2. (a) SEM image of the dry pre-compressed foam with the Rise/swelling Direction of the foam RD perpendicular to the page; (b) SEM image of the dry pre-expanded foam with RD perpendicular to the page; (c) SEM image of the dry pre-compressed foam with RD as shown; (d) SEM image of the dry pre-expanded foam with RD as shown; (e) Schematic of the two scales of the porosity in pre-expanded foam; (f) Optical image of the dry and partially wet pre-expanded cellulose foam.

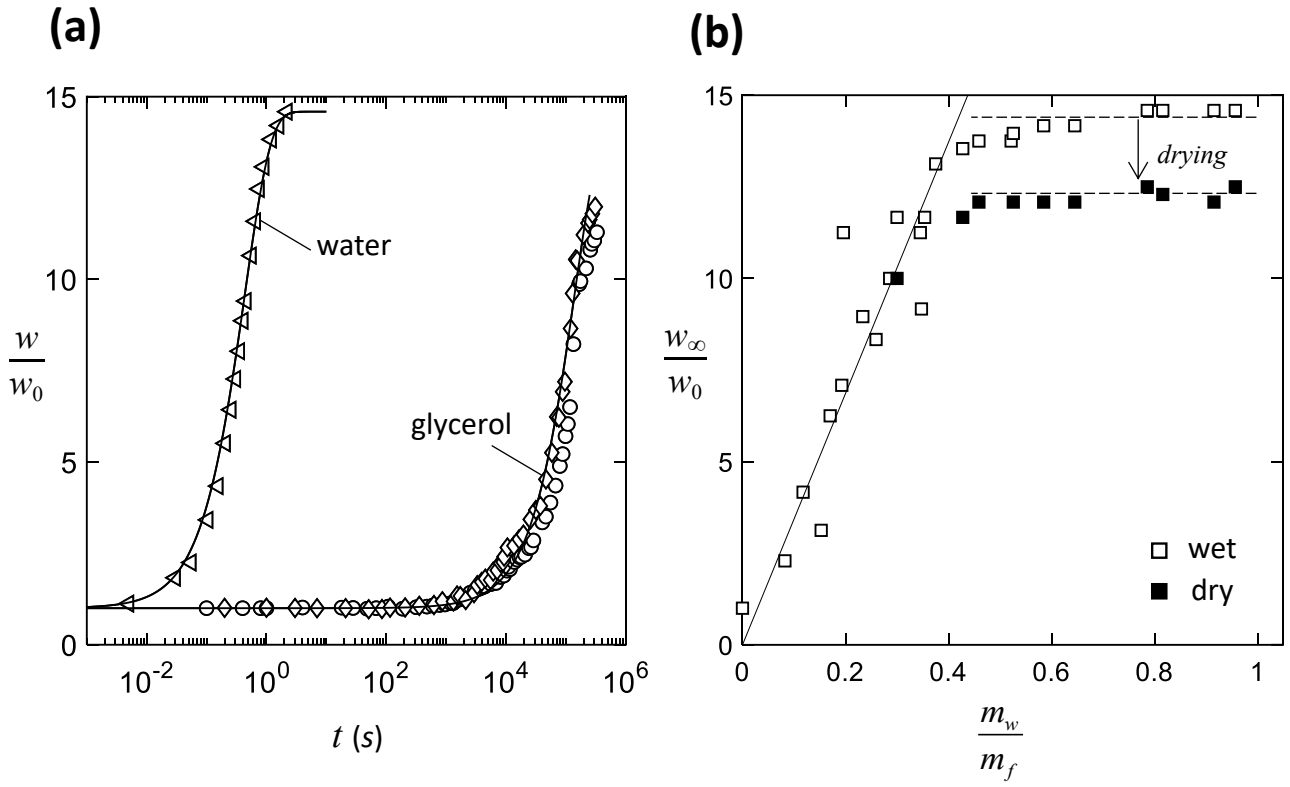

Fig. 3. (a) Measured swelling stretch factor w/w_0 with time t for the immersion of the pre-compressed foam in water and glycerol, where w is the time-dependent thickness of the foam in the rise/swelling direction and w_0 = 2.4 mm is the initial thickness of the foam in rise/swelling direction. The solid lines show the fitted curve $w/w_0 = 1 + \alpha\left[1 - \exp(-t/\tau)\right]$, where α = 13.6 and τ = 0.436 s for water and τ = 1.4 × 10^5 s for glycerol. (b) Measured swelling stretch factor w_∞ / w_0 at long time versus water content m_w / m_f. The measured normalized swelling factor upon drying is shown as filled symbols.

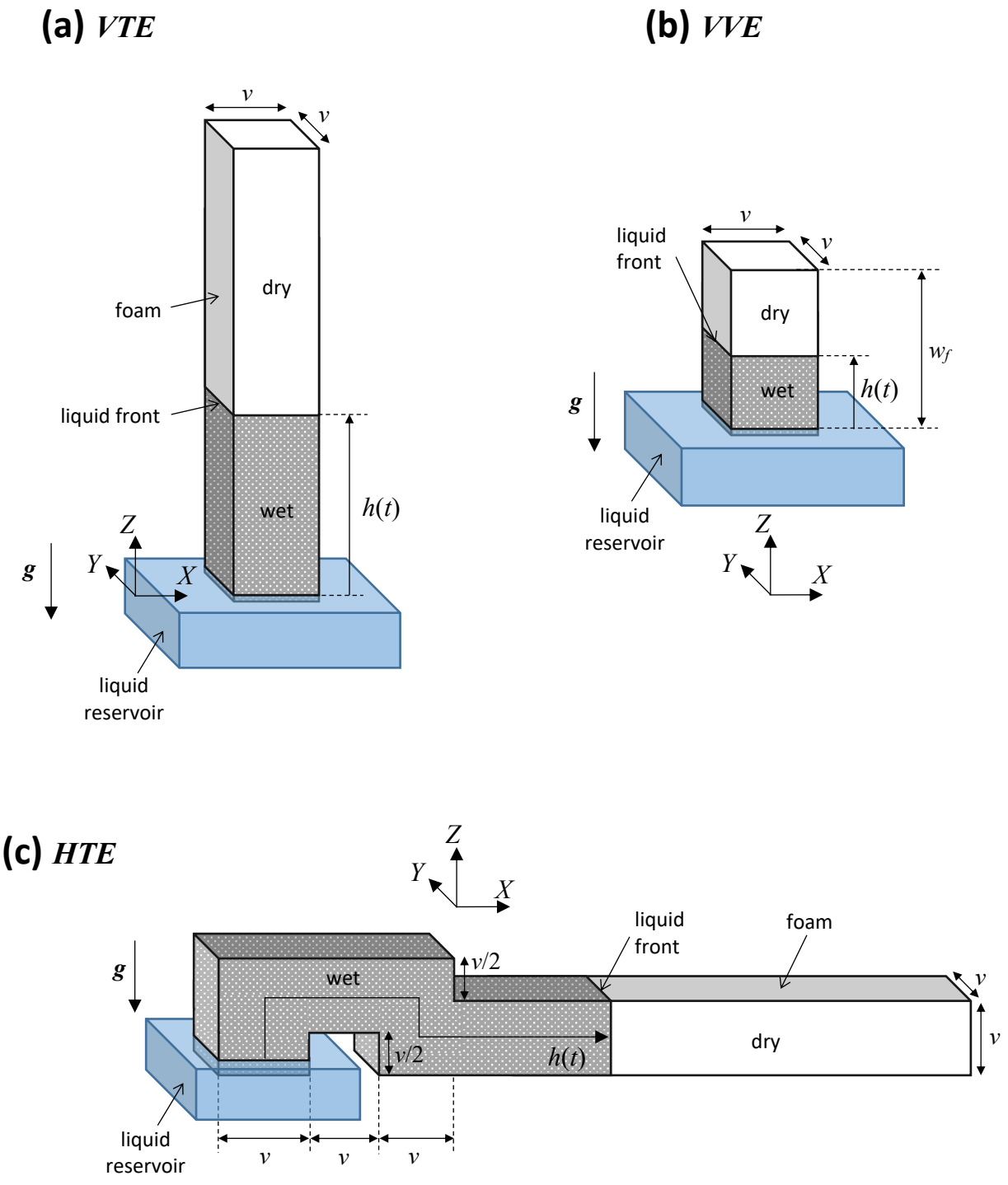

Fig. 4. (a) Test geometry for the vertical reservoir-fed test with the Rise/swelling Direction RD of the foam in transverse direction for the pre-expanded foam (VTE); (b) Test geometry for the vertical reservoir-fed test with the RD in the flow direction for the pre-expanded foam (VVE); (c) Test geometry for the horizontal reservoir-fed test with the RD in the transverse direction for the pre-expanded foam (HTE).

(a) ***VTC***

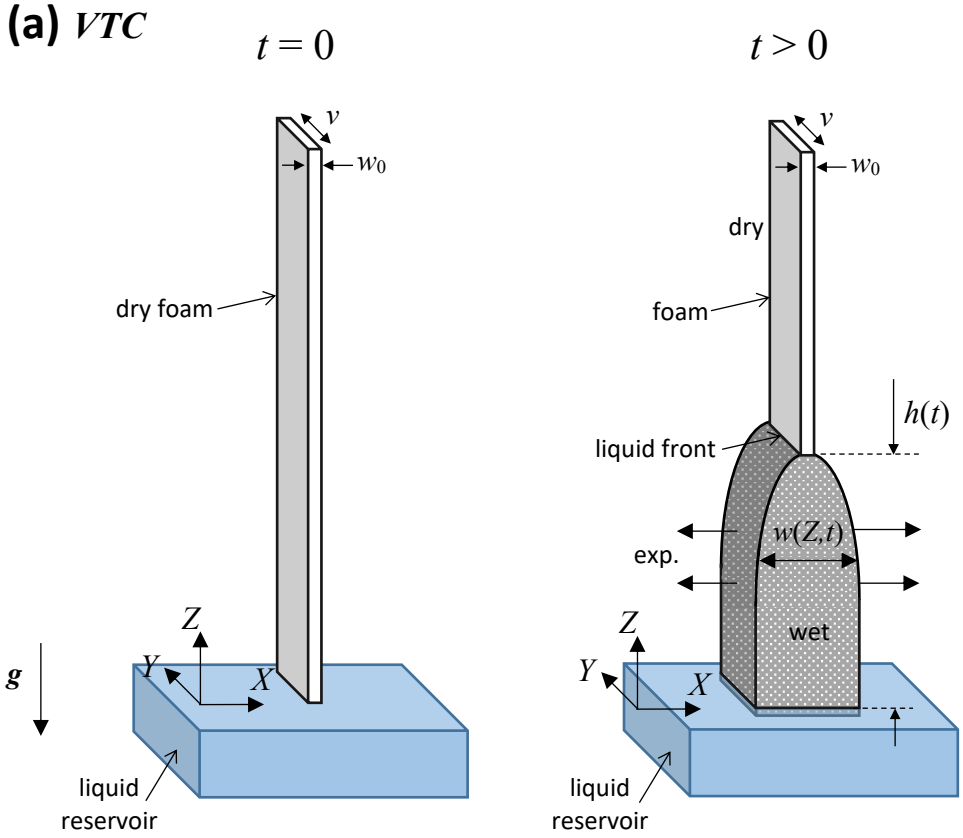
t = 0
t > 0
v
w0
dry foam
dry
foam
h(t)
liquid front
w(Z,t)
exp.
wet
Z
Y
X
g
liquid reservoir

(b) ***VVC***

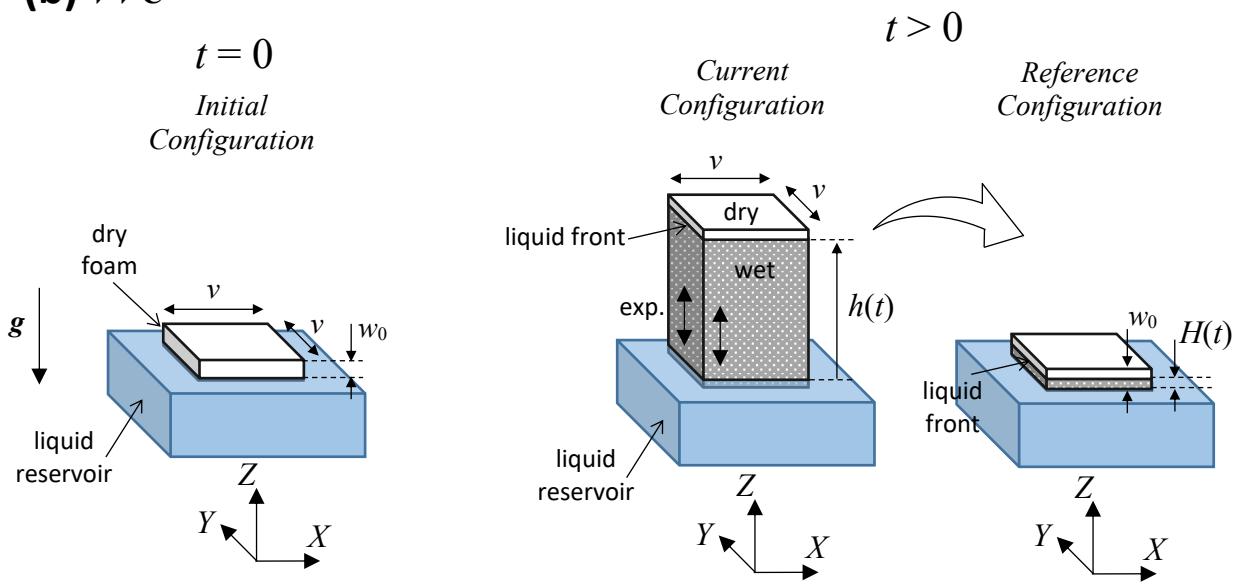
t = 0
Initial Configuration
t > 0
Current Configuration
Reference Configuration
dry foam
v
w0
g
liquid reservoir
liquid front
dry
wet
exp.
h(t)
H(t)
Z
Y
X

(c) *HTC*

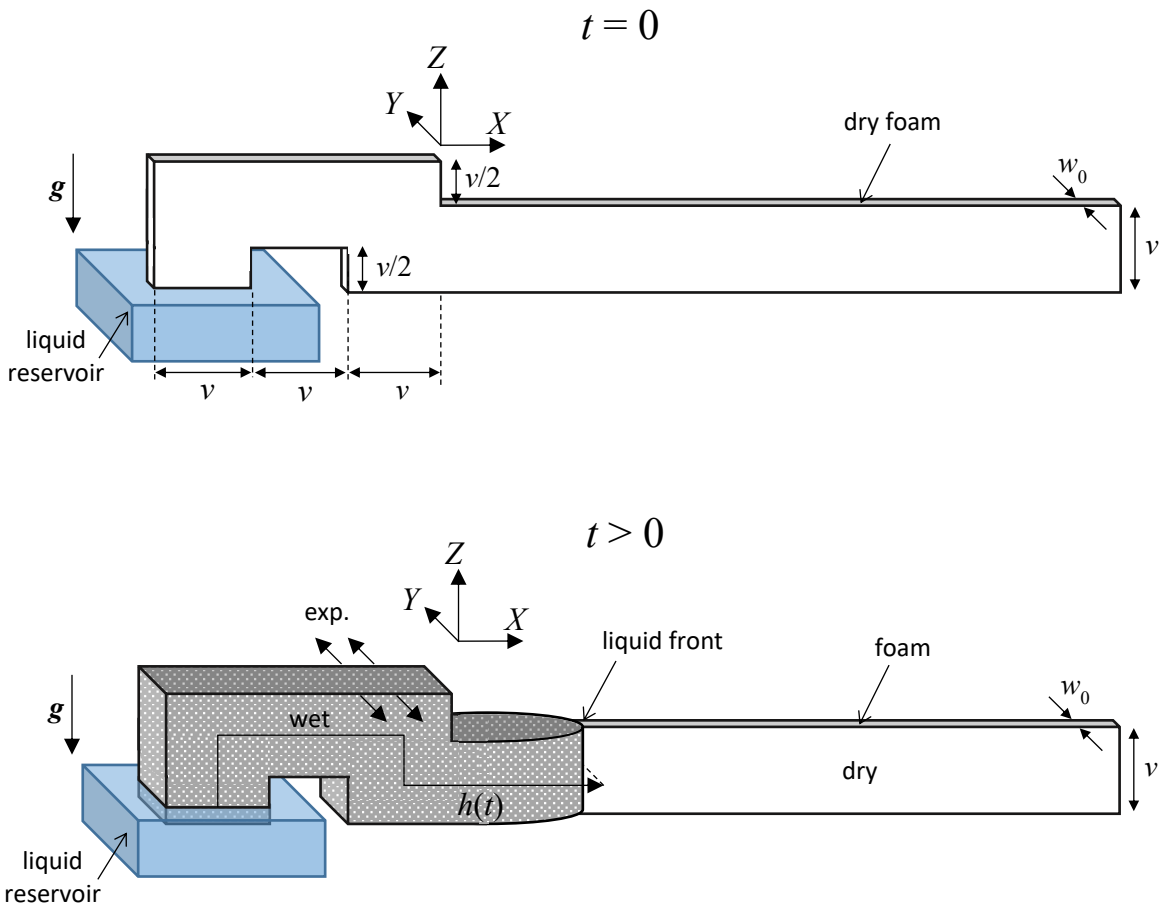

Fig. 5. (a) Test geometry for the vertical reservoir-fed test with the Rise/swelling Direction RD of the foam in transverse direction for the pre-compressed foam (VTC); (b) Test geometry for the vertical reservoir-fed test with the RD in the flow direction for the pre-compressed foam (VVC); (c) Test geometry for the horizontal reservoir-fed test with the RD in the transverse direction for the pre-compressed foam (HTC).

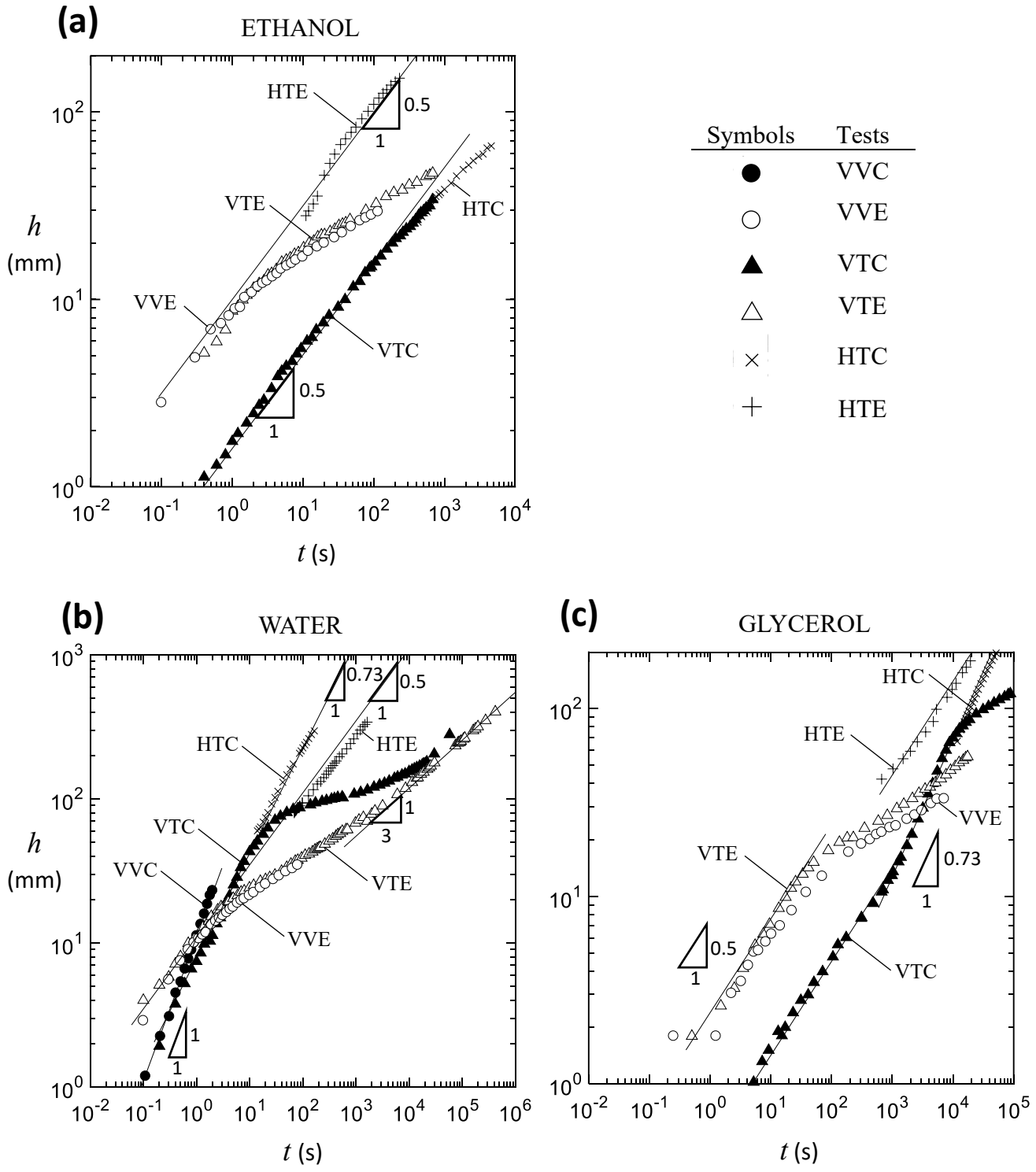

Fig. 6. Measured liquid front length *h* versus time *t* for the pre-compressed and pre-expanded foams for different test arrangements with respect to the flow direction and the rise/swelling direction RD of the foam using (a) ethanol, (b) water and (c) glycerol.

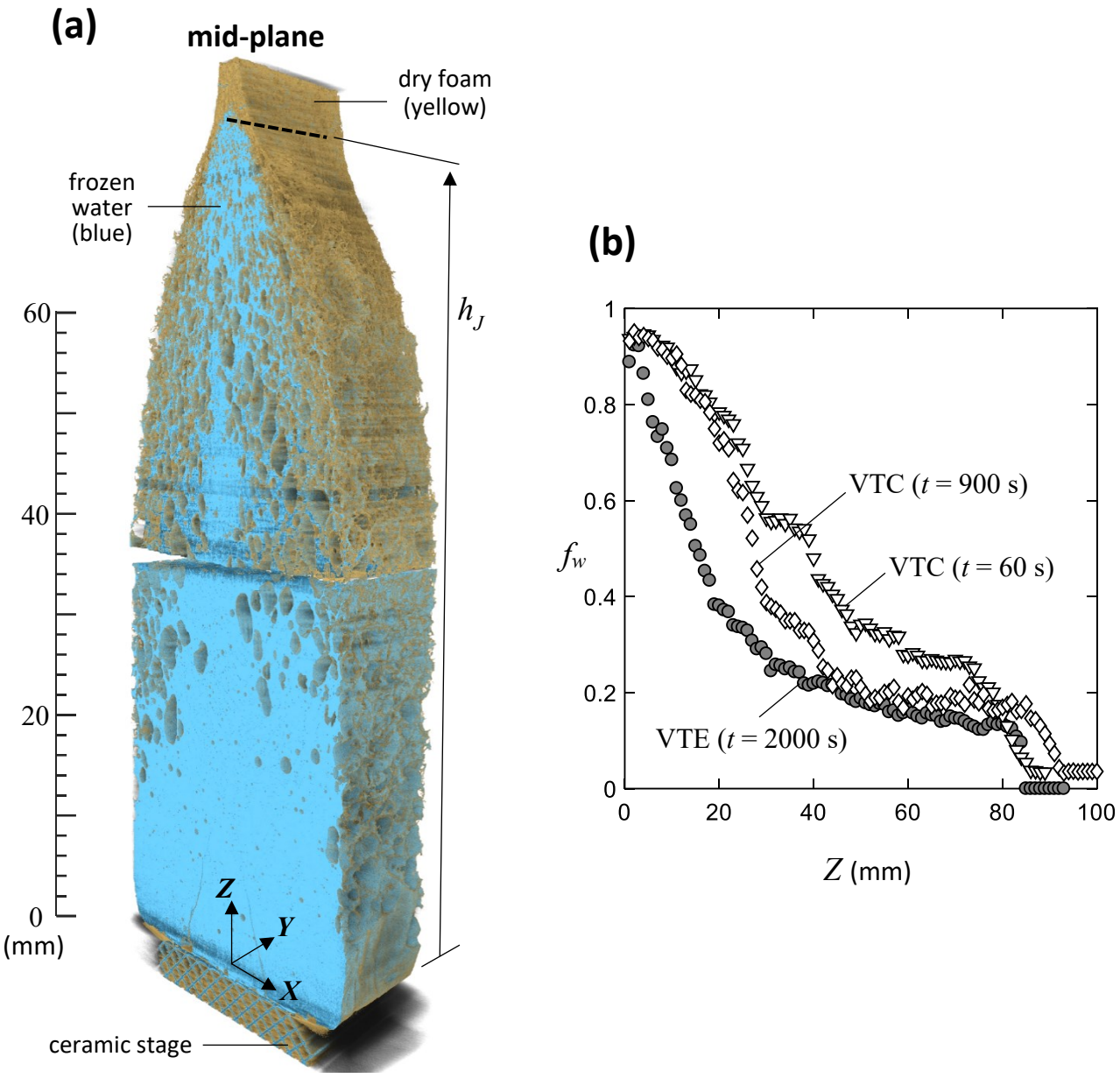

Fig. 7. (a) The 3D reconstructed computed tomography X-ray image of the pre-compressed cellulose foam during the VTC water reservoir-fed test at t = 60 s; (b) Measured volume fraction of water f_w in the VTC test versus position Z at time t = 60 s and t = 900 s compared with the volume faction of water f_w profile in the VTE test at time t = 2000 s.

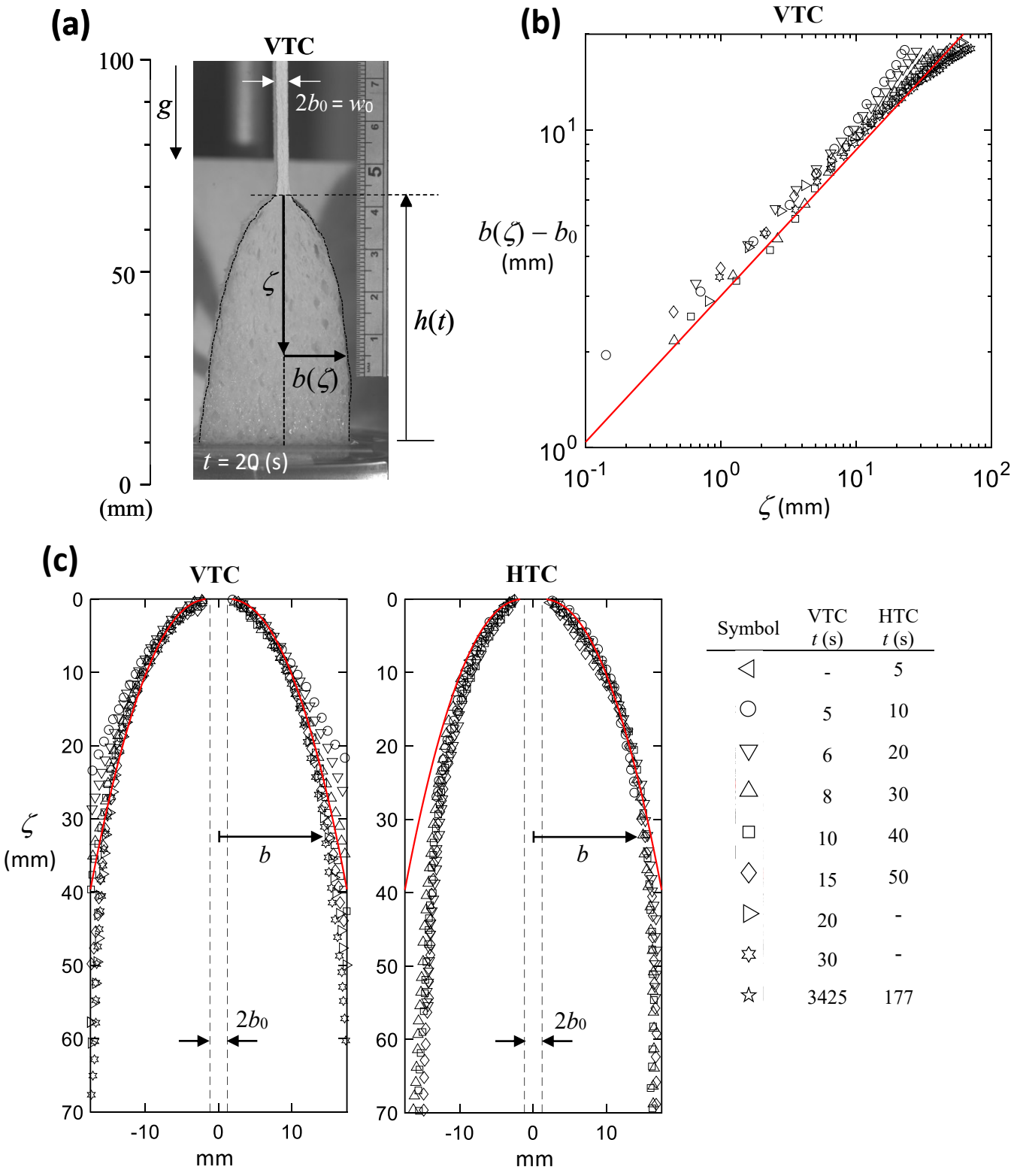

Fig. 8. (a) Image of the pre-compressed foam upon water rise in the VTC test. (b) Measured swelling profiles of the foam versus coordinate ζ during the water rise in the VTC test at selected times. (c) Measured swelling profiles of the pre-compressed foam for the water rise in the VTC and HTC tests at selected times in a true scale plot: solid lines show the fitted curve given in (b).

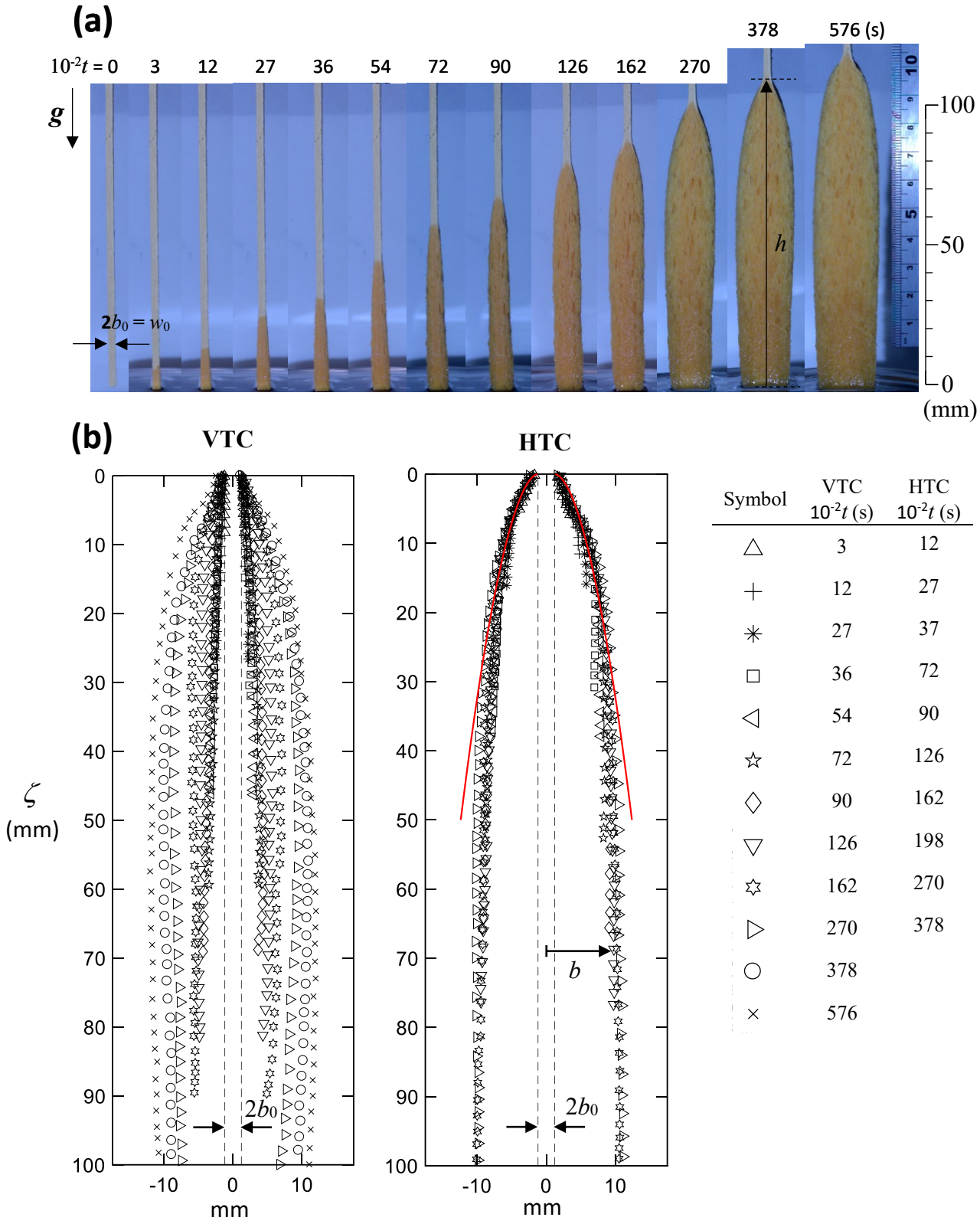

Fig. 9. (a) Sequential images of the pre-compressed foam during the glycerol rise in the VTC test; (b) Measured swelling profile of the pre-compressed foam in glycerol rise in the VTC and HTC tests at selected times.

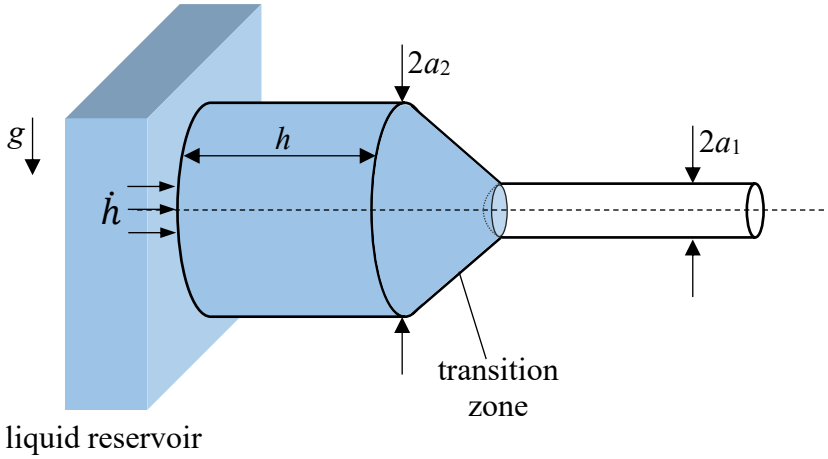

Fig. 10. Sketch of horizontal capillary flow in a swelling tube.

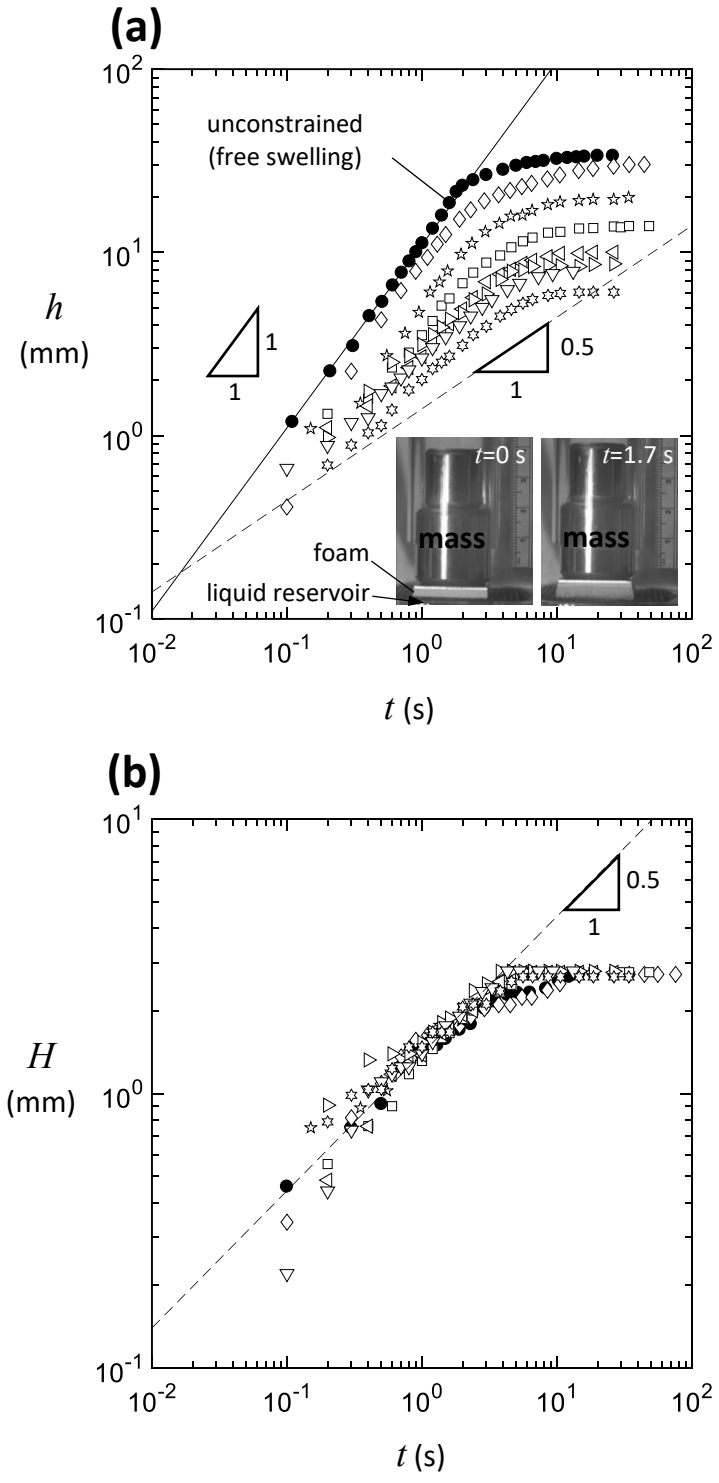

Symbols	Restraining pressure, p_0 (kPa)
●	0 (free swelling)
◇	0.40
☆	0.98
□	1.6
◁	2.4
▷	3.7
▽	5.1
✡	9.2

Fig. 11. (a) Measured water front height h versus time t in the constrained VVC tests for selected values of compressive pressure p_0. (b) Wet front height in the un-deformed configuration of the foam H versus time t in the constrained VVC tests (see Fig. 5b).

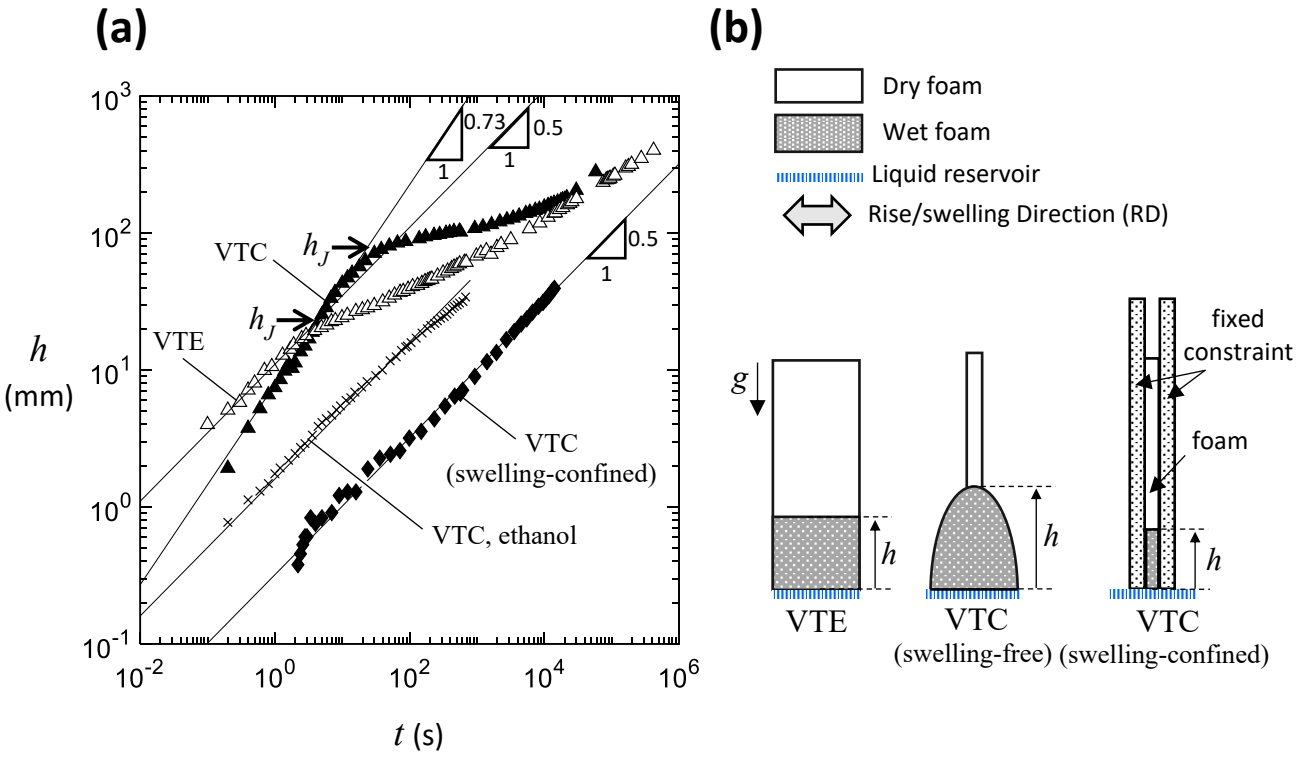

Fig. 12. (a) Measured wet front height *h* with time *t* for the VTE, VTC and swelling confined VTC reservoir-fed tests; (b) A sketch of the VTE, swelling-free VTC and swelling-confined VTC reservoir-fed tests.